2014 IEEE 11th International Conference on Mobile Ad Hoc and Sensor Systems

SmartSensing: Sensing Through Walls with Your Smartphone!

Yongpan Zou[§†], Guanhua Wang[†], Kaishun Wu[‡*], Lionel M. Ni[†‡]
[§] Xi'an Jiaotong University
[†]Department of Computer Science and Engineering, Hong Kong University of Science and Technology
[‡]Guangzhou HKUST Fok Ying Tung Research Institute
[*]College of Computer Science and Software Engineering, Shenzhen University
{yzouad,gwangab,kwinson,ni}@cse.ust.hk

***Abstract*—Seeing through walls and knowing clearly what exist inside just like a superman are not only fantastic wishes for humans, but also of much practical significance. For example, you would like to know whether there are pipes, or rebars inside a wall before drilling into it. Moreover, knowing how pipes are configured in a wall before attempting to fix defects would definitely prevent unnecessary damages. Existing methods that intend to address this issue are either costly due to the use of high-end technology, or too restrictive for reasons of some strong assumptions. However, in this paper, we present a novel system, SmartSening, which is based on off-the-shelf sensors embedded in smartphones. SmartSensing makes full use of in-built sensors, namely, the accelerometer, the gyroscope, and the magnetometer to achieve this goal inexpensively and conveniently. Specifically, by combining these sensors, we are able to clearly distinguish certain objects inside a wall. In addition, the layout of a pipeline system can be mapped out automatically in an economical and labour-saving way. We implement this system on two different kinds of smartphone platforms, namely iPhone4 and Xiaomi Mi2S. We conduct experiments in a proof-of-concept testbed of size 1.8m×1.0m. Experimental results show that SmartSensing can achieve no less than an average accuracy of 96%, 89% and 77% in distinguishing objects under three different depths, respectively. Also, as for layout mapping, it can achieve less than 32cm and 28cm length error with 90% probability on average for whole horizontal and vertical pipeline segments, with a 6.8m and 4.0m total length, respectively.**

I. Introduction

Obtaining a perspective of a wall is not just an adolescent fantasy inspired by the movie *Superman*. More importantly, it has great practical significance as well. Nowadays, as space efficiency and aesthetics are increasingly taken into consideration for interior design, in-wall pipeline systems for water supply and draining have become continually popular [1]. What is more, modern architects prefer reinforced concrete structures for fastness. However, inconvenience even dangers can arise when drilling through a wall for practical purposes like repairing defective pipes due to existing in-wall structures. Hitting a rebar while drilling into a wall can destroy the drill itself and severely weaken the concrete structure. In the case where an in-wall layout is unknown, repairing pipes even with just a few defects can become destructive and labour-intensive work [2]. All these add up to to absolute necessity of gaining a view of in-wall structures.

Previous work aims at achieving the goals mentioned above can mainly be divided into two parts–distinguishing hidden objects, and mapping hidden systems' layouts especially for pipeline systems. For the first part, some high-end technologies like Ground-penetrating radar (GPR) [3] and multi-sensor technology are adopted whether in research work [4] or commercial products [5][6], at the price of easy access and high cost. As for hidden layout mapping, previous work either holds some strong assumptions which limits its practical use [7], or makes use of sophisticated equipment which makes them not so commonly available [4][8]. However, this paper presents SmartSensing, a smartphone-based application that achieves the goals of detecting and distinguishing certain objects hidden inside a wall, and further mapping a pipeline layout. By taking advantage of off-the-shelf smartphones, SmartSensing avoids utilizing specialized tools, and has relatively high scalability as well.

SmartSensing is based on the fact that ferromagnetic materials like irons, steels and iron-containing alloies can distort a local geomagnetic field and cause local magnetic anomalies. As a result, when a magnetometer is moving close to such kind of objects, any abnormal responses induced by local magnetic anomalies can be detected. What is more, local magnetic anomalies induced by a kind of ferromagnetic object is closely related to the object itself [9][10][11], which can be used to differentiate in-wall objects [12][13].

Specifically, SmartSensing works in two main modes: distinguishing in-wall objects and mapping pipeline layout. In the former mode, a smartphone scans across a wall and detects the magnetic anomaly if an object exists. At the same time, by making use of displacement information acquired by motion sensors (i.e., accelerometer and gyroscope), unique profiles of local magnetic anomaly can be built for the detected objects, which can then be used for distinguishing them. In the mapping pipeline layout mode, we focus on the pipes hidden in a wall. In a similar way, when the smartphone scans across a wall repeatedly, an increasing number of the points where pipes traverse can be located on the wall by combining the accelerometer and the gyroscope. After that, by applying a simple curve reconstruction method, the pipeline layout can be reconstructed automatically by SmartSensing.

The idea is straightforward; nevertheless, several challenges need to be solved in order to implement SmartSensing.

First, how to calculate displacement accurately when moving a smartphone over the wall? Accurate displacement is not only necessary for constructing unique profiles for object-

978-1-4799-6036-1/14 $31.00 © 2014 IEEE
DOI 10.1109/MASS.2014.46

distinguishing purpose, but also indispensable for locating points where pipes traverse for later mapping the layout. Although accelerometer-based methods have been proposed for distance estimation, however, they are not appropriate for our application on account of their relatively high errors.

Second, how to distinguish different objects? It is very intuitive to think that objects can be distinguished by the magnetic intensity metric. Actually, the previous study [14] and our simple magnetic survey in the apartment declare it to be unreliable and misleading, since the spatial variance of an indoor magnetic field is large.

Third, how to map the pipeline layout automatically? Suppose accurate positions of points where pipes traverse can be obtained, it is non-trivial to connect them correctly for automatically mapping the pipeline layout. To address this problem, we propose a simple curve reconstruction method by applying certain constraints, considering practical application scenarios.

Summary of results: we design and implement SmartSensing on two different smartphone platforms: iPhone4 and Xiaomi Mi2S. Both platforms contain sensors of different types and parameters. The results show that SmartSensing can distinguish three common in-wall objects with no less than an average accuracy of 96%, 89% and 77% under three different depths, i.e., 5cm, 7cm, 9cm, respectively. In addition, the overall mapping error for a pipeline system of a total length of 10.8m is less than 60cm with a probability of 90%.

To sum up, this paper's main contributions are as follows:

- By introducing a special movement, and carefully calibrating acceleration and velocities, this work accomplishes accurate displacement calculation. Based on that, in-wall objects can be distinguished and located.
- We transform the in-wall pipeline layout mapping problem into a problem of connecting points in a plane correctly, which can be solved by a simple proposed method. By this means, some strong assumptions required by previous work can be relaxed.
- Instead of utilizing additional sensors or any specialized tools, we implement SmartSensing on two smartphone platforms. Experiments conducted in a proof-of-concept testbed show that SmartSensing can distinguish three kinds of objects with high accuracy, and map out the in-wall pipeline layout with low errors.

The rest of this paper is organized as follows. Section II presents the related work. Section III presents how to calculate the displacement accurately. Section IV presents the way to distinguish different objects and locate points that an object pass through. Section V describes the experimental setup. Section VI shows the experimental results and evaluates the performance. Section VIII conducts discussions about SmartSensing. Section IX concludes this work.

II. Related Work

As a smartphone-based application intened to accmoplish detecting/distinguishing hidden objects and map out pipeline system's layout, SmartSensing is closely related to previous work mainly in two aspects: detecting/distinguishing hidden objects; mapping hidden facilities' layouts.

Detecting/Distinguishing hidden objects: As for detecting/distinguishing hidden objects, different technologies based on various principles are proposed. Commercial products like metal detectors and wall scanners [5][6] are available for household applications such as detecting electrical wires or metal objects inside a wall before hammering in a nail or drilling into the wall. The methods adopted by these commercial products usually involve radar technology, which detects and distinguishes objects by analyzing reflected signals. However, differences between these products and SmartSensing are conspicuous mainly in two aspects. First, commercial products employ expensive and specialized tools to achieve accurate distinguishing ability, and thus rendering them not as economical and easily available as SmartSensing. Also, commercial products do not involve automatic mapping of in-wall pipeline layouts, while SmartSensing can accomplish this easily by the combination of motion sensors and magnetometer in a smartphone.

Mapping hidden pipeline layout: As for mapping the layout of hidden utilities, Mapping the Underworld [4] is aimed at mapping out underground infrastructures by means of electromagnetic induction and UWB radar technology. The Pipeline Pigging method is introduced in detail in [8]. In this method, multiple sensors are mounted on a mechanical pig. As the "pig" walks through the whole pipeline system, data of pipelines such as lengths, locations of intersections and defects are collected for later analysis. Although they can achieve relatively comprehensive and high-precision information about pipelines, the specilized tools and sophisticated system designs they employ tremendously hinder their household application. By comparison, SmartSensing does not make use of any specialized tools and sophisticated system design which dramatically reducing the cost and increasing the portability, and can achieve considerable performance for household applications. Another work closely related to SmartSensing is [7], which also aims at mapping out the in-wall pipeline layout. In contrast, [7] utilizes a tiny mobile sensor capsule in which a pressure sensor and a gyroscope are enclosed, to traverse the whole pipeline and collect data to construct the topology of the pipeline system. However, this method has several restricted conditions: the diameter of pipes should be constant and big enough; also, since large amounts of possible paths from entrances to exits exist in a given pipeline system, repeated trials are inevitable. These requirements limit its application in practical scenarios.

III. Displacement Calculating

For Smartsensing, accurate displacement is essential either for building profiles of different objects, or pinpointing points through which pipes pass. Theoretically, for a smartphone-based application, displacement can be calculated via accelerations by:

$$Dis(t) = Dis_0 + v_0 t + \int \int_0^t a(t) dt d\tau \tag{1}$$

Where $Dis(t)$ is the displacement at instant t, Dis_0 is the initial placement, v_0 is the initial velocity, $a(t)$ is the acceler-

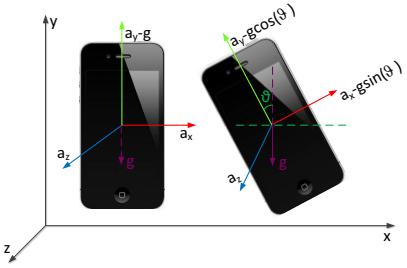

Fig. 1. Gravity projected on a smatphone due to its rotation.

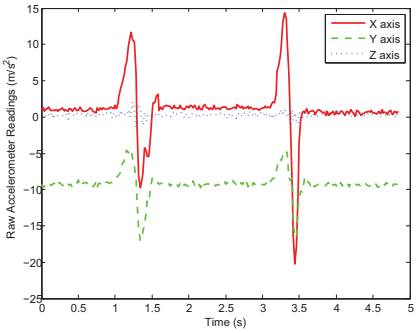

Fig. 2. Raw accelerometer readings during two strokes.

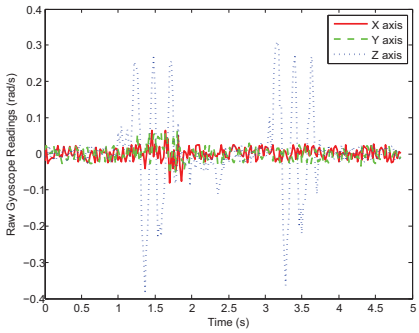

Fig. 3. Raw gyroscope readings during two strokes.

ation.

The above formula goes for continuous situation, while for the discrete case, it can be modified to:

$$Dis(i) = Dis(i-1) + \frac{v(i-1)+v(i)}{2}\Delta t \tag{2}$$

Where $v(i) = v(i-1) + \frac{a(i)+a(i-1)}{2}\Delta t$.

Actually, accelerometer-based methods are adopted for velocity even distance estimation in indoor navigation or localization [15][16] and for moving pattern analysis [17][18]. However, these methods mainly apply to coarse-grained distance calculation at the price of accuracy. When acceleration is simply integrated twice, errors caused by interference and measurements will be accumulated twice correspondingly and eventually result in ugly displacement results.

In order to mitigate errors of displacement calculation, a special movement–stroke is adopted. A stroke is a short period of rapid movement beginning and ending in a stationary state. Between consecutive strokes, a short pause is intentionally set for the purpose of calibration. The rationale of introducing stroke movements is two-fold. First of all, the relatively high acceleration of a stroke is beneficial for reducing errors caused by measurements. Secondly, the relatively short duration of a stroke introduces less interference caused by a usr's involuntary hand jitters. Further more, in our application, it is reasonable to assume that movements of a smartphone are limited in a plane, since this can easily be accomplished by moving the smartphone against a wall. Nevertheless, directly integrating the acceleration is never a wise choice, that is, careful calibration and correction should be done on acceleration and velocity before each integration.

A. Dealing with hand rotation

Problem: smartphones are commonly equipped with a 3-axis accelerometer and a 3-axis gyroscope which can measure linear acceleration and rotational speed in X, Y and Z direction, respectively. However, as the accelerometer is very sensitive to gravity, any rotation of the smartphone will cause an additive component of gravity on each axis. As a result, the accelerometer readings will not only contain the actual acceleration of the stroke movement, but will also incorporate the projected gravity component, as shown in Fig.1. Unfortunately, it is difficult to move a smartphone without rotation resulting from wrist movement even in a short stroke. Fig.2 and Fig.3 show the raw accelerometer and gyroscope readings in two consecutive strokes.

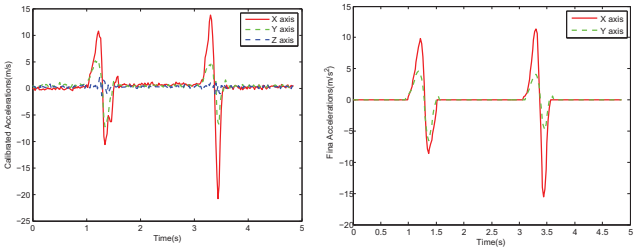

(a) Calibrated acceleration by gyroscope (b) Final processed acceleration

Fig. 4. Calibration of Acceleration

Solution: pauses between strokes are utilized for calibration. That means, each time we move a smartphone to scan a wall, during the pause period, the rotation angle θ of the smartphone can be calculated [19]:

$$\theta = arctan(\frac{a_x}{a_y}) \tag{3}$$

where, a_x, a_y are the accelerometer readings in X and Y direction respectively. After obtaining θ, it is easy to calibrate the accelerometer readings before proceeding with next stroke by:

$$a'_x = a_x + g\sin\theta \tag{4}$$

$$a'_y = a_y + g\sin\theta \tag{5}$$

As for rotation happening during each stroke, since the rotation angle cannot be obtained by (3), gyroscope is made use of to detect the rotation and calculate the rotation angle by:

$$\theta' = \int g_z(t)dt \tag{6}$$

where, $g_z(t)$ represents gyroscope readings during a stroke.

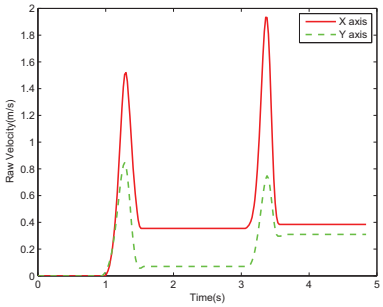

Fig. 5. Raw velocity by integrating acceleration .

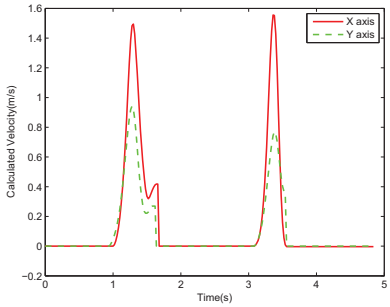

Fig. 6. Final processed velocity.

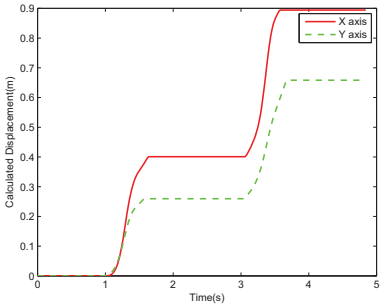

Fig. 7. Final calculated displacement.

B. Dealing with hand vibration

It is noted that as the movement of the smartphone is limited in a vertical plane, the rotation can only happen around the Z axis. Therefore, only Z-axis gyroscope readings are utilized for acceleration calibration using (4) and (5) just by substituting θ for θ', a_x for a'_x and a_y for a'_y. Fig.4a shows the calibrated acceleration by subtracting the gravity components in X and Y axes.

Problem: accelerometers are very sensitive to even minor movement caused by hand vibrations. Although calibration using a gyroscope removes the gravity component in raw acceleration, jitters caused by hand vibrations remain. Consequently, it is necessary to remove this background noise in order to gain accurate acceleration values.

Solution: in regard to noise caused by hand vibration, firstly, a moving average filter is applied to smooth the calibrated acceleration. The moving average filter is the most common filter in DSP, not only because of its simplicity of use, but also because it is an optimal tool for reducing random noise while retaining a sharp step response [20]. Then we set a threshold for acceleration based on the mean value of acceleration when the smartphone is held stationary. Readings below the threshold will be regarded as background noise and set to zeros. Fig.4b shows the result after this step.

C. Dealing with velocity drift

Problem: after obtaining the cleaned accelerations, intuitively, displacement can be computed directly by applying (1). However, by doing so the result is still rather inaccurate. Errors in acceleration will reflect in the velocity after integrating the acceleration. That is, for a single stroke, ideally the velocity should start from zero and end at zero. However, this rule is usually disobeyed due to even a single unexpected impulse in acceleration and would eventually cause the final velocity to be a constant instead of zero, as shown in Fig.5. As a result, this velocity drift ultimately brings about large error in displacement calculation.

Solution: the method we adopted for solving the velocity drift problem is using a moving window of size 5 operated on the velocity which we obtained by integration. Velocity readings will be set to zeros if consecutive velocity gradients in a window are all zeros. The key insight is that consecutive constant velocity usually indicates that the smartphone is held stationary, instead of being moved. By applying this method, velocity drift will be suppressed. Fig.6 and Fig.7 show the final processed velocity and calculated displacement, respectively.

IV. Objects Distinguishing

A. Basics of geo-magnetic field

Generally, the term "magnetic field" can refer to a magnetic B field or a magnetic H field. These two fields are distinct but closely related, in vacuum:

$$B = \mu_0 H \tag{7}$$

where μ_0 is the magnetic constant ($4\pi \times 10^{-7}$Vs/Am). However, when there is magnetic material, the relationship of these two magnetic fields can be expressed as:

$$B = \mu_0 \mu_r H \tag{8}$$

Where μ_r is the relative permeability of the magnetic material.

As magnetic B field reveals the real cause of the magnetic field, it is more commonly used for describing a magnetic field [21]. The units of B is Tesla(T) or Gauss(G) (1T=10^4G). A magnetic field can be habitually described by seven non-independent parameters: declination(D), inclination (I), horizontal intensity(H), vertical intensity(Z), the north(X) and east(Y) components of the H, and total intensity(F), as shown in Fig.8. The total intensity of the geomagnetic field at the earth's surface varies from 23 Gauss to 66 Gauss [22].

Magnetic field intensity can be measured by two types of magnetometers: vector sensors and total field sensors [23]. The former measures a single component of the magnetic induction. That is, for a vector magnetometer, $B_x, B_y,$ and B_z are all obtained. However, for the latter, it only measures the magnitude of the field without its direction. The total field intensity can be obtained from the vector magnetometer:

$$B_{total} = \sqrt{B_x^2 + B_y^2 + B_z^2} \tag{9}$$

Where B_x, B_y, B_z are magnetic intensity component along X, Y and Z axis in Fig.8.

Earth's undistorted magnetic field in a small-scale region will be of a constant magnitude and direction, since the magnetic gradient of the geomagnetic field is 10nT/km. However, when a ferrous object like an alloy steel, a cast iron, or a steel reinforcement of panel is present in the geomagnetic field, the object will become magnetized by the primary magnetic

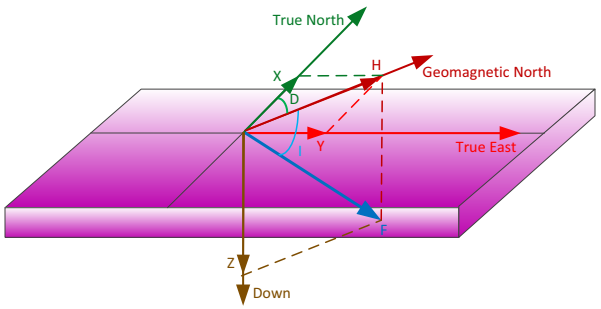

Fig. 8. Description of magnetic field.

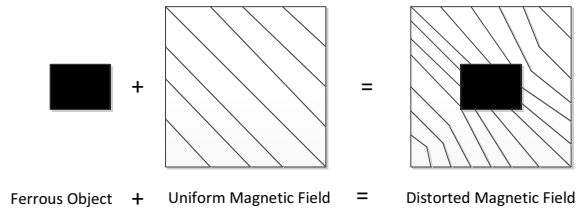

Fig. 9. Distorted magnetic field caused by ferromagnet.

field (i.e., geomagnetic field) and induce a secondary magnetic field. The resulting field is a combination of the primary and secondary fields. As a result, the local magnetic field will be distorted as shown in Fig.9, and consequently creates magnetic anomalies in the resultant magnetic field which can be detected by magnetometer. Based on the anomalies detected by a magnetometer, hidden objects can be detected.

B. Distinguishing and Locating objects

As reported in [14], an indoor geomagnetic field presents noticeable spatial variance even on a small scale due to the steel shells in most modern buildings. This spatial variance can be used to aid indoor localization as done in [24] [25]. However, it will cause difficulties for detecting and distinguishing objects based on the intensity metric, especially when the magnetic anomalies caused by objects are relatively tiny. However, the key insight we obtain is that by introducing the stroke movement, the whole relatively long scanning process is divided into several small parts (20cm-50cm) and spatial variance in this small region is negligible compared with the anomaly caused by an object(such as a pipe, a rebar and etc.). This can be made use of to detect the presence of an object.

Further, we ask such a question: *can we distinguish objects instead of just detecting them simply by our smartphones?* A straightforward idea is comparing the maximal intensity of magnetic anomalies, since intuitively objects with stronger magnetism cause stronger magnetic anomalies. Although this idea is simple, it does not work well in practical scenarios. The primary reason is that since spatial variance of indoor magnetic fields exists as described above, the intensity of magnetic anomalies caused by even the same object in different positions may not be the same. As a result, the maximal-intensity metric fails to satisfy the goal of distinguishing objects reliably.

The idea of solving this problem is inspired by magnetic field theory [26]. When a magnetometer crosses over a certain ferromagnetic object, the magnetic anomalies detected by the magnetometer present a certain relation with the displacements between the object and magnetometer. In addition, different objects present different relations between magnetic anomalies and displacements, which can be viewed as unique profiles of objects as reported in [27]. Since displacements when moving a smartphone can be acquired as described in Section III, obtaining magnetic profiles of different objects is a relatively easy task. We simply need to combine the displacement obtained by motion sensors with the magnetic anomalies detected by the magnetometer to construct profiles. However, a metric should

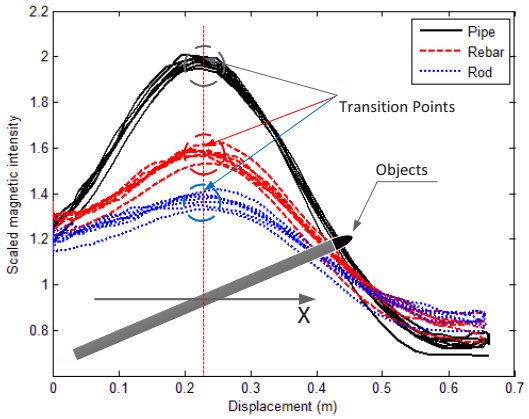

Fig. 10. Magnetic Profiles for Pipe,Rebar & Rod.

be proposed for distinguishing objects based on profiles. Considering the computational overhead, we utilize a simple but effective metric–curve similarity to distinguish different objects. Each time we move the smartphone across objects, the profiles of objects will be acquired, and their similarities will be calculated to distinguish objects. The similarity is defined by:

$$d(X,Y) = \sqrt{\sum_{i=1}^{n}(x_i - y_i)^2} \tag{10}$$

$$Sim(X,Y) = \frac{1}{1+d(X,Y)} \tag{11}$$

Where $X = (x_1, x_2, ..., x_n)$, $Y = (y_1, y_2, ..., y_n)$ represents the scaled magnetic anomalies of different objects as shown in Fig.10. $Sim(X,Y)$ is the similarity between two profiles. It is noted that for this similarity mertic, equal number of samples are required for two profiles. However, this cannot be always satisfied in practical scenarios as sampling time and rate may be different. This issue can be handled by linear interpolation [28].

Obtaining the profile of an object not only allows us to distinguish objects, but also enables us to locate the points where an object (like a pipe, a rebar, or a rod) traverses on a wall. This can be accomplished from the obtained profile of a detected object, since the magnetic anomalies and displacements are both recorded as shown in Fig.10. The only

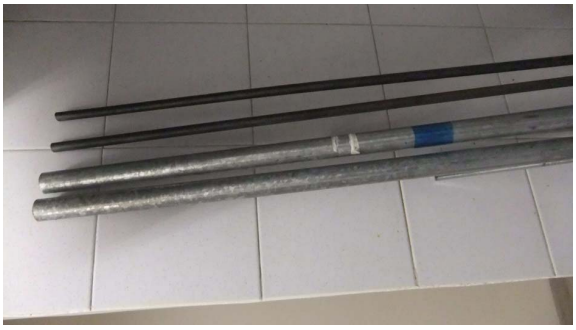

Fig. 11. Galvanized steel pipes, reinforcing rebars and iron rods used for experiments.

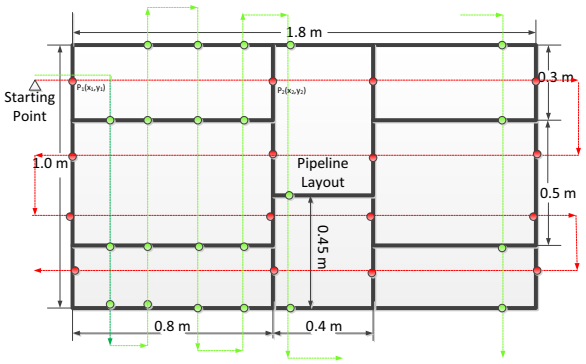

Fig. 12. Pictorial description of Pipeline layout for the experiment and traces of scanning the wall.

thing should be done is to decide which point in the curve corresponds to the point where a pipe traverse accurately. The principle we use for this purpose is to pinpoint the point in the curve where the magnetic intensity goes through a transition as shown in Fig.10.

V. Mapping Layout

As mentioned above, when we move a smartphone across a wall, the points where pipes traverse can be located. As positions of these points can be obtained and stored at the same time in this process, large number of points can be acquired when scanning times are increased. All these points indicate the positions of pipes. Therefore, by deliberately connect them, the layout of a hidden pipeline system can be uncovered. This mapping process can be reduced to a curve reconstruction problem, which is defined informally as: given a set of sample points on a smooth curve in a plane, the problem of connecting them according to their adjacencies on the curve is called the curve reconstruction problem [29][30]. However, as for our application, classical curve reconstruction algorithms are excessively powerful and also complex since a simple method can be applied by considering practical constraints of an in-wall pipeline layout.

The first constraint that can be made use of is that the pipeline layout in a wall usually contains only vertical and horizontal segments for the convenience of installation and water flowing [2]. Another constraint is that the shortest pipe segment in a pipeline system is usually not too short, say longer than 20cm in our scenario. Considering these two constraints, the following method is proposed for mapping the layout.

Step 1: Horizontally scan across the wall, and make sure that the vertical distance between the adjacent horizontal scanning traces is less than 20cm, as shown in the red lines in Fig.12. After scanning, points set $P^R = ((x_1^R, y_1^R), (x_2^R, y_2^R), ..., (x_n^R, y_n^R))$, where (x_i^R, y_i^R) represents the coordinate of a point relative to the starting point, can be obtained (red points in Fig.12).

Step 2: Vertically scan across the wall, and make sure that the horizontal distance between the adjacent vertical scanning traces is less than 20cm, as shown in the green lines in Fig.12. After scanning, points set $P^G = ((x_1^G, y_1^G), (x_2^G, y_2^G), ..., (x_n^G, y_n^G))$ can be obtained (green points in Fig.12).

Step 3: Sort the points set P^R based on x first. Compare adjacent points' x. If the difference is less than a threshold Δx, the adjacent points are classified into the same group, otherwise, they belong to different groups. For each group, sort the points based on y and compare adjacent points' y, if the difference is less than a threshold Δy, they stay in the same group; otherwise, split them into different groups. Connect points in each group with a vertical line segment, whose X position is the mean value of points' x in this group. After this step, the vertical pipe segments can be mapped out. Applying a similar way to points set P^G, the horizontal pipe segments can be mapped out.

Step 4: Combine the vertical segments and horizontal segments to form a raw layout. Extend line segments in the layout until both ends of each segment intersect with other line segments.

It is noted that the time complexity of the above method is dominated by sorting, thus a $O(n \lg n)$ efficiency where n is the number of points can be expected. It is obvious that the accuracy of layout mapping highly depends on the points we obtain in the scanning process. The more points we get, the more accurate the layout mapping will be, but at the cost of intensive labor. As a result, a trade-off should be made between scanning effort and difficulty of mapping.

VI. Experiments Setup

We implement SmartSensing on the iPhone4 and Xiaomi Mi2S platforms. We use a proof-of-concept testbed to evaluate the functions of SmartSensing. Components of this testbed include galvanized steel pipes (external diameter: 25mm, inner diameter: 19mm), reinforcing rebars (diameter: 10mm) and iron rods (diameter: 7mm) which commonly exist in the walls of modern buildings. Also, a wall of 9cm thickness and slates of different thicknesses (7cm and 5cm, respectively) are also used for the experiments. The reason we use slates is that we need to investigate the influence of depth on distinguishing objects hidden in a wall (also considering the difficulty of finding proper walls for experiments). For convenience of description, the wall and slates used in the experiments are uniformly referred to as walls. Experiments are carried out in three

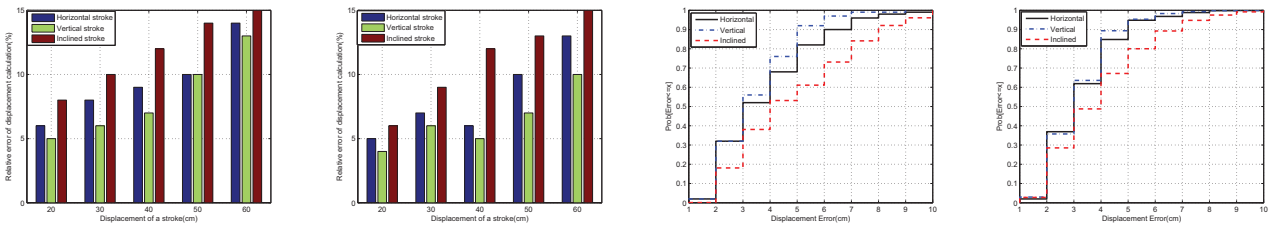

(a) Displacement errors VS stroke length for iPhone.

(b) Displacement errors VS stroke length for Mi2S.

(c) CDFs of displacement errors for iPhone.

(d) CDFs of displacement errors for Mi2S.

Fig. 13. Distance calculation performance for two smartphones in different scenarios.

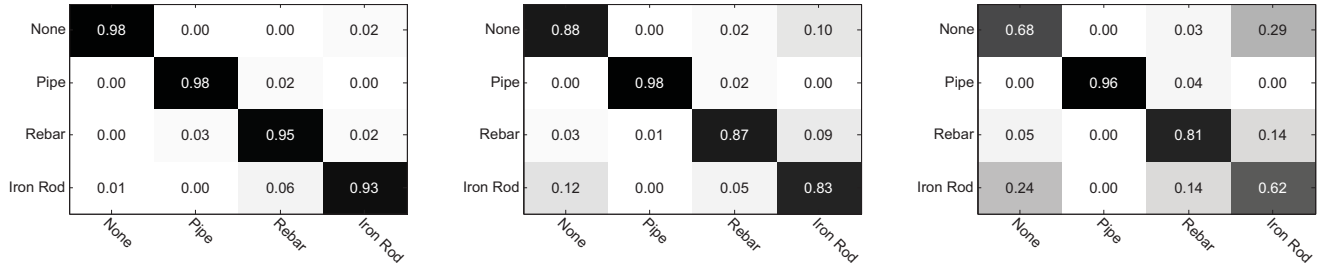

(a) wall thickness=5

(b) wall thickness=7

(c) wall thickness=9

Fig. 14. iPhone's performance of distinguishing objects under different wall thicknesses.

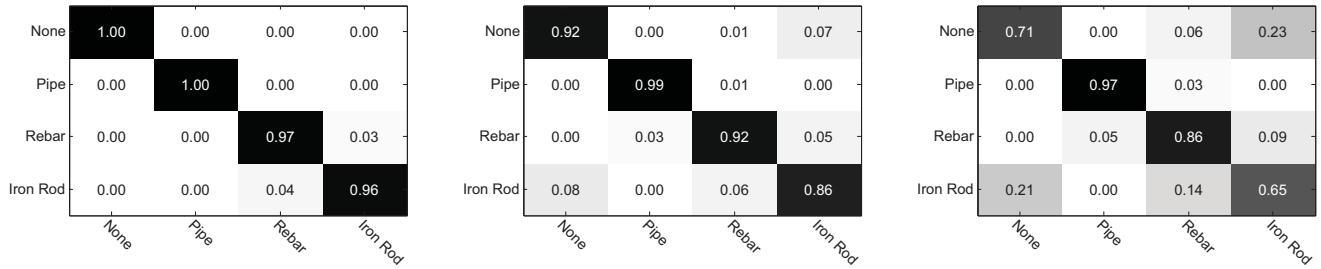

(a) wall thickness=5

(b) wall thickness=7

(c) wall thickness=9

Fig. 15. Xiaomi's performance of distinguishing objects under different wall thicknesses.

different sections: experiments to test displacement-calculating accuracy, experiments to test the object-distinguishing accuracy and experiments to test the layout-mapping accuracy.

In the first section, our goal is to evaluate the performance of the displacement calculating method. We conduct three types of experiments: moving a smartphone horizontally, vertically and obliquely. Each time volunteers are asked to move the smartphone against the wall in a certain way (horizontally, vertically or obliquely) at a certain displacement. When a stroke is completed, the displacement will be computed correspondingly. Compared with the ground truth, relative errors are acquired. We conduct the experiments for 20 times in each case (horizontally, vertically or obliquely and different displacements) for each volunteer (10 volunteers in total).

In the second section, the objective of the experiments is to test the accuracy of distinguishing objects buried under different depths. Galvanized steel pipes, reinforcing rebars and iron rods are put closely behind each wall mentioned above. A smartphone is moved across the wall to identify what exactly is behind the wall for a number of times at different locations in the apartment. According to the similarities caculated, objects can be distinguished and the corresponding accuracies can be obtained by comparing with the ground truths.

In the third section, a pipeline layout as shown in Fig.12 is used for our experiments. In this layout, each segment represents a galvanized steel pipe which is commonly used in household plumbing system. A smartphone scans across the wall on the other side and pinpoints the points a pipe segment traverses. Each time, the scanning process startes from the same point , which is useful for coordinate transformation from the wall to the smartphone. After several times of scanning, enough points can be obtained and the pipeline layout is mapped out via the method described in Section V. A total

number of 200 repeated experiments are conducted on the testbed using iPhone4 and Mi2S by different volunteers.

VII. Evaluation

A. Displacement-Calculating Accuracy

Fig.13a and Fig.13b plot the displacement errors in each scenario as a function of displacement of each stroke for iPhone4 and Xiaomi Mi2S. Fig.13c and Fig.13d plot cumulative density functions (CDFs) of displacement errors for a vertical movement (the red line), a horizontal movement (the green line) and a resultant movement (the blue line), when the displacement of each stroke is optionally chosen. The results reveal several facts: (1) the displacement calculation error is closely related to the displacement of each stroke. it increases with the displacement of a stroke. This is because when the displacement of each stroke increases, it is harder for one to move a smartphone in a controlled movement as required. It indicates that it is better to move a smartphone by no more than (40-50)cm in each stroke. (2) the vertical strokes cause less errors than the horizontal ones. This is because the horizontal strokes usually accompany with more rotation due to the wrist movement than vertical strokes. Although the rotation movement can be calibrated via the gyroscope, this will also lead to some errors. (3) for 90% cases, less than 6cm displacement error can be achieved for both horizontal and vertical movements for iPhone4 platform, and less than 5cm error can be achieved for Mi2S platform.

B. Objects-distinguishing Accuracy

Fig.14 shows the object-distinguishing performance of iPhone4 platform under different wall thicknesses. As shown in the figure, an average accuracy of 96%, 89% and 77% can be obtained when the thickness of the wall is 5cm, 7cm and 9cm, respectively. When the wall thickness increases, the overall performance will degrade as expected, especially for rebar and iron rod. In addition, it is easiest to differentiate the galvanized steel pipe, yet hardest to differentiate the an iron rod, especially when the wall thickness increases. The reason is that the magnetic anomaly caused by a galvanized steel pipe is much more obvious to be distinguished than that caused by an iron rod.

Fig.15 shows the performance of Mi2S platform. Similarly, the overall trends in performances are similar to the results of iPhone4 platform. However, compared with iPhone4, Mi2S have a slightly better performance in distinguishing objects. This is maybe because of a little more remarkable capabilities of the embedded sensors.

C. Layoyut Mapping Accuracy

In order to evaluate the performance of pipeline layout mapping, we choose pipe length errors as the evaluation metric. In practice, we compare total lengths of horizontal and vertical pipe segments of the real layout with those of the reconstructed one. Fig.16 shows the CDFs of the length errors of both horizontal and vertical segments after multiple experiments. It shows that a less than 32cm error can be obtained with a probability of 90% for horizontal pipes which have a 6.8m total length, and an less than 28cm error can be obtained with a probability of 90% for vertical pipes which have a 4.0m total length. It demonstrates that SmartSensing can gain a satisfying performance in mapping layout.

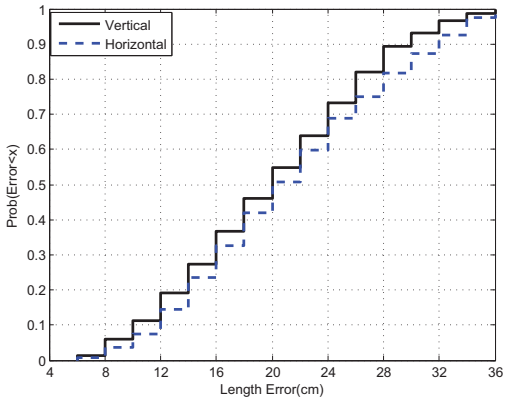

Fig. 16. Layout-Mapping Accuracy.

VIII. Discussion

It is noted that so far we only claim that SmartSensing can just work for 2D scenarios. That is, SmartSensing can detect and distinguish objects in a plane, and can only map out a pipeline system which is configured over two dimensions. However, we prudently calim that 2D scenarios can cover alomost all household in-wall systems.

In the current version of SmartSensing, in order to mitigate errors of displacement calculations, we introduce a special movement–stroke, which requires users to move a smartphone in a highly controlled way and consequently brings about a certain degree of inconvenience for users. Considering the user experimence, more complicated and sophisticated methods such as complementary filtering, direction cosine matrix and etc. can be applied for displacement calculation and orientation estimation in the future work such that accurate displacement calculation can be accomplished without controlling the way of moving a smartphone.

In the mapping layout stage, in order to figure out the layout of a in-wall pipeline system, enough points where pipes traverse should be located on the wall. It is noted that our layout reconstruction method applies to the case where scanning process across a wall is conducted horizontally and vertically. Improvements can be done in layout reconstruction algorithm so as to remove this constraint. What is more, another interesting question is that whether we can find an optimally method to scan across a wall in order to reduce scanning effort but can also obtain enough points for layout reconstructing. We leave this as a future work in order to make SmartSensing more attractive.

IX. Conclusion

In this paper, we propose a novel system SmartSensing based on off-the-shelf smartphones to distinguish certain objects hidden in the wall. What is more, SmartSensing can be used to map the pipeline layout hidden in a wall automatically by just scanning across the wall. Experimental results from our proof-of-concept testbed measuring 1.8m$\times$1.0m show that:

first, for the purpose of distinguishing objects, SmartSensing running on an iPhone4 can achieve an overall accuracy of 96%, 89% and 77% when the wall thickness is 5cm, 7cm, and 9cm, respectively. SmartSensing running on a Mi2S can achieve an overall accuracy of 98%, 92% and 80%, respectively; second, for pipeline layout mapping purpose, 90% of the errors are less than 32cm for total horizontal pipe segments with a total legth of 6.8m, and 90% of the errors are less than 28cm for total vertical pipe segments with a total length of 4.0m. By combining the in-built multiple sensors, that is, the accelerometer, the gyroscope and the magnetometer, we avoid utilizing specialized devices or tools, but can achieve practical functions as well.

X. ACKNOWLEDGEMENTS

This research is supported in part by Program for New Century Excellent Talents in University (NCET-13-0908), HKUST16207714, Guangdong Natural Science Funds for Distinguished Young Scholar (No.S20120011468), New Star of Pearl River on Science and Technology of Guangzhou (No.2012J2200081), China NSFC Grant 61202454.

REFERENCES

[1] A. Massey, *Interior of the twentieth century*, New York, 1990.

[2] M. M, G. H, and M. M. A, *Pipeline design and construction: a practical approach*. New York: ASME press, 2000.

[3] D. J. Daniels, *Ground penetrating radar*. Iet, 2004, vol. 1.

[4] MappingUnderworld, http://www.mappingtheunderworld.ac.uk.

[5] WallScanner, http://www.boschtools.com/Products/Tools/Pages/BoschProductDetail.aspx?pid=GMS120.

[6] RadarScannerKit, http://www.dewalt.com/tools/cordless-instruments-radar-scanning-dct418s1.aspx.

[7] T. ted Lai, Y. han (Tiffany) Chen, P. Huang, and H. hua Chu, "Pipeprobe: a mobile sensor droplet for mapping hidden pipeline," in *Proceedings of the 8th ACM Conference on Embedded Networked Sensor Systems*, 2010.

[8] T. J. N. H., "Pipeline pigging technology," *Gulf Professional Publishing*, 1992.

[9] C. E., "Magnetization of steel building materials and structures in the natural geomagnetic field," *Acta Polytechnica*, vol. 45, no. 6, pp. 47–52, 2005.

[10] A. J and Z. B. G., "Magnetic anomaly detection in ferromagnetic material," in *PIERS Proceedings*, 2011.

[11] B. Larry and J. E. Rocchio, "Magnetic surveying for buried metallic objects," *Ground Water Monitoring and Remediation*, 1990.

[12] M. J. E., Y. Das, and R. O. Ellingson, "Locating and identifying compact ferrous objects," *IEEE Transactions on Geoscience and Remote Sensing*, vol. 28, no. 2, pp. 182–193, 1990.

[13] M. J. E, B. M, D. B, C. R. H, and Y. Das.s, "A magnetostatic signature measurement and analysis system," *Journal of Physics E: Scientific Instruments*, vol. 18, no. 1, 1985.

[14] L. Binghao, G. Thomas, D. A. G, and R. Chris, "How feasible is the use of magnetic field alone for indoor positioning?" in *Proceedings of IEEE 2012 International Conference on Indoor Positioning and Indoor Navigation (IPIN)*, 2012.

[15] G. Pang and H. Liu, "Evaluation of a low-cost mems accelerometer for distance measurement," *Journal of Intelligent and Robotic Systems*, vol. 30, no. 3, pp. 249–265, 2001.

[16] P. Zhuang, D. Wang, and Y. Shang, "Smart:simultaneous indoor localization and map construction using smartphones," in *Neural Networks(IJCNN), The 2010 International Joint Conference on Neural Networks*. IEEE, 2010, pp. 1–8.

[17] F. Foerster and J. Fahrenberg, "Motion pattern and posture: correctly assessed by calibrated accelerometers," *Behavior research methods, instruments, & computers*, vol. 32, no. 3, pp. 450–457, 2000.

[18] K. Sagawa, H. Inooka, and Y. Satoh, "Non-restricted measurement of walking distance," in *Systems, Man, and Cybernetics, 2000 IEEE International Conference on Systems, Man, and Cybernetics*, vol. 3. IEEE, 2000, pp. 1847–1852.

[19] P. Mohan, V. N. Padmanabhan, and R. Ramjee, "Nericell: rich monitoring of road and traffic conditions using mobile smartphones," in *Proceedings of the 6th ACM conference on Embedded network sensor systems*. ACM, 2008, pp. 323–336.

[20] Smith and S. W., "The scientist and engineer's guide to digital signal processing," 1997.

[21] C. Sydney and B. Julius, *Geomagnetism*. Oxford: Clarendon Press, 1940.

[22] S. Maus, S. Macmillan, S. McLean, B. Hamilton, A. Thomson, M. Nair, and C. Rollins, *The US/UK World Magnetic Model for 2010-2015*. West Mains Road ,Edinburgh EH9 3LA ,UK: NOAA National Geophysical Data Center, 2010.

[23] J. Lenz and A. S. Edelstein, "Magnetic sensors and their applications," *Sensors Journal, IEEE*, vol. 6, no. 3, pp. 631–649, 2006.

[24] C. Jaewoo, D. Matt, S. Chris, K. Ig-Jae, R. Pedram, and W. Micaela, "Indoor location sensing using geo-magnetism," in *Proceedings of the 9th international conference on Mobile systems, applications, and services*, 2011.

[25] A. Michale, F. Martin, D. Marek, J. B. J., and R. Patrick., "Characterization of the indoor magnetic field for applications in localization and mapping," in *Indoor Positioning and Indoor Navigation (IPIN), 2012 International Conference on Indoor Positioning and Indoor Navigation. IEEE*, 2012.

[26] J. E. Mcfee, R. Ellingson, and Y. Das, "A total-field magnetometer system for location and identification of compact ferrous objects," *Instrumentation and Measurement, IEEE Transactions on Instrumentation and Measurement*, vol. 43, no. 4, pp. 613–619, 1994.

[27] J. E. McFee, R. Ellingson, J. Elliott, and Y. Das, "Estimation of depth, orientation, length and diameter of long, horizontal ferrous rods using a fluxgate magnetometer," DTIC Document, Tech. Rep., 1993.

[28] E. Meijering, "A chronology of interpolation: from ancient astronomy to modern signal and image processing," *Proceedings of the IEEE*, vol. 90, no. 3, pp. 319–342, 2002.

[29] N. Amenta, M. Bern, and D. Eppstein, "The crust and the β-skeleton: Combinatorial curve reconstruction," *Graphical models and image processing*, vol. 60, no. 2, pp. 125–135, 1998.

[30] T. K. Dey, K. Mehlhorn, and E. A. Ramos, "Curve reconstruction: Connecting dots with good reason," in *Proceedings of the fifteenth annual symposium on Computational geometry*. ACM, 1999, pp. 197–206.